PUBLICATIONS OF THE ASTRONOMICAL SOCIETY OF THE PACIFIC, **113**:353–361, 2001 March

PISCES: A Wide-Field, 1–2.5 μm Camera for Large-Aperture Telescopes[1]

D. W. MCCARTHY, JR.,[2] J. GE,[3] J. L. HINZ,[4] R. A. FINN,[5] AND R. S. DE JONG[6]

Steward Observatory, 933 North Cherry Avenue, Tucson, AZ 85721

Received 2000 May 26; accepted 2000 November 7

ABSTRACT. Wide-field-of-view infrared cameras, operating on the new generation of large telescopes, offer unprecedented gains in the detection of faint sources and in observing efficiency for both direct imaging and spectroscopy. With a 1024 × 1024 pixel, 1–2.5 μm detector, the PISCES camera provides 8.′5 and 3.′16 fields at the 2.3 m Bok telescope and 6.5 m Multiple Mirror Telescope, respectively. Its refractive optics utilize all spherical surfaces and standard glasses. A cold pupil stop suppresses the thermal background produced by the emissive surfaces normally present in Cassegrain optical configurations. The optical design is directly extendable to wider fields with larger detector formats. Future upgrades include low-resolution (R = 200–500) multiobject spectroscopy.

1. INTRODUCTION

Large-format (1024 × 1024, 2048 × 2048 pixel) near-infrared detector arrays allow astronomers to map wide-angle structures and to survey broad areas of the sky with unprecedented efficiency and sensitivity. With a large field of view, astronomers can avoid the photometric inaccuracies and operational overheads associated with mosaicking many smaller frames obtained over several nights, possibly under different sky conditions. Imaging and multiobject spectroscopy of star formation regions, Kuiper Belt objects, stellar populations in external galaxies, galaxy clusters, and quasar environments are just a few examples of astronomical observations that profit from wide-field instruments. Such observations are especially powerful with the large apertures of modern 6.5–10 m diameter telescopes.

PISCES is a wide-field imager in use on both the Bok 2.3 m telescope, providing a field of 8.′5 diameter, and the 6.5 m Multiple Mirror Telescope (MMT), with a field of 3.′16 diameter. Through accurate pupil reimaging and cold baffling, PISCES blocks the thermally emissive structures associated with the f/9 Cassegrain foci of these telescopes. Here we describe the optical-mechanical design (§ 2), detector characteristics (§ 3), control system (§ 4), wide-field data reduction (§ 5), and astronomical performance (§ 6) of this camera.

2. OPTICAL-MECHANICAL DESIGN

PISCES (Fig. 1) can reimage the focal plane from any telescope with an f-ratio ≥9 onto its HAWAII (1024 × 1024 pixel) detector (Kozlowski et al. 1994; Hodapp et al. 1996). The optical design, shown in Figure 2, uses six lenses with spherical surfaces. Table 1 summarizes the specific optical prescription. Except for the dewar window, all optical elements are cooled to 77 K by liquid nitrogen. For the 2.3 m Bok reflector and 6.5 m MMT at f/9, the final f-ratios are f/3.3 and f/3.18, respectively, yielding fields of view of 8.′5 and 3.′16 in diameter with plate scales of 0.″5 and 0.″185 pixel^{-1}.

2.1. Requirements

PISCES was built as a test bed for a Rockwell HAWAII detector which had been procured for eventual use in an adaptive optics instrument under construction for the 6.5 m MMT (Sarlot et al. 1999). A suitable dewar, shown in Figure 3, was already available from the former FASTTRAC instrument (Close & McCarthy 1994) with optics designed for diffraction-limited imaging. These optics were replaced for this new wide-field application.

The optical design of PISCES was constrained by the following five considerations. First, to conserve costs in dewar modifications and optics, a circular field of view was chosen to fit within the 1024 × 1024 pixel detector format. Second, a pixel scale of 0.″5 pixel^{-1} was chosen to provide Nyquist sampling of the typical seeing disk at the 2.3 m telescope. Third, spot sizes were optimized for the K band, but seeing-limited performance was also desired in the J and H bands. Fourth, since the 2.3 m telescope is not optimized for low background operation at its f/9 Ritchey-Chrétien Cassegrain focus, the optics were designed to reimage the pupil onto a

[1] Observations reported here were obtained at the MMT Observatory, a joint facility of the University of Arizona and the Smithsonian Institution.

[2] dmccarthy@as.arizona.edu.

[3] Current address: Department of Astronomy and Astrophysics, Pennsylvania State University, University Park, PA 16802; jian@astro.psu.edu.

[4] jhinz@as.arizona.edu.

[5] rfinn@as.arizona.edu.

[6] Hubble Fellow; rdejong@as.arizona.edu.

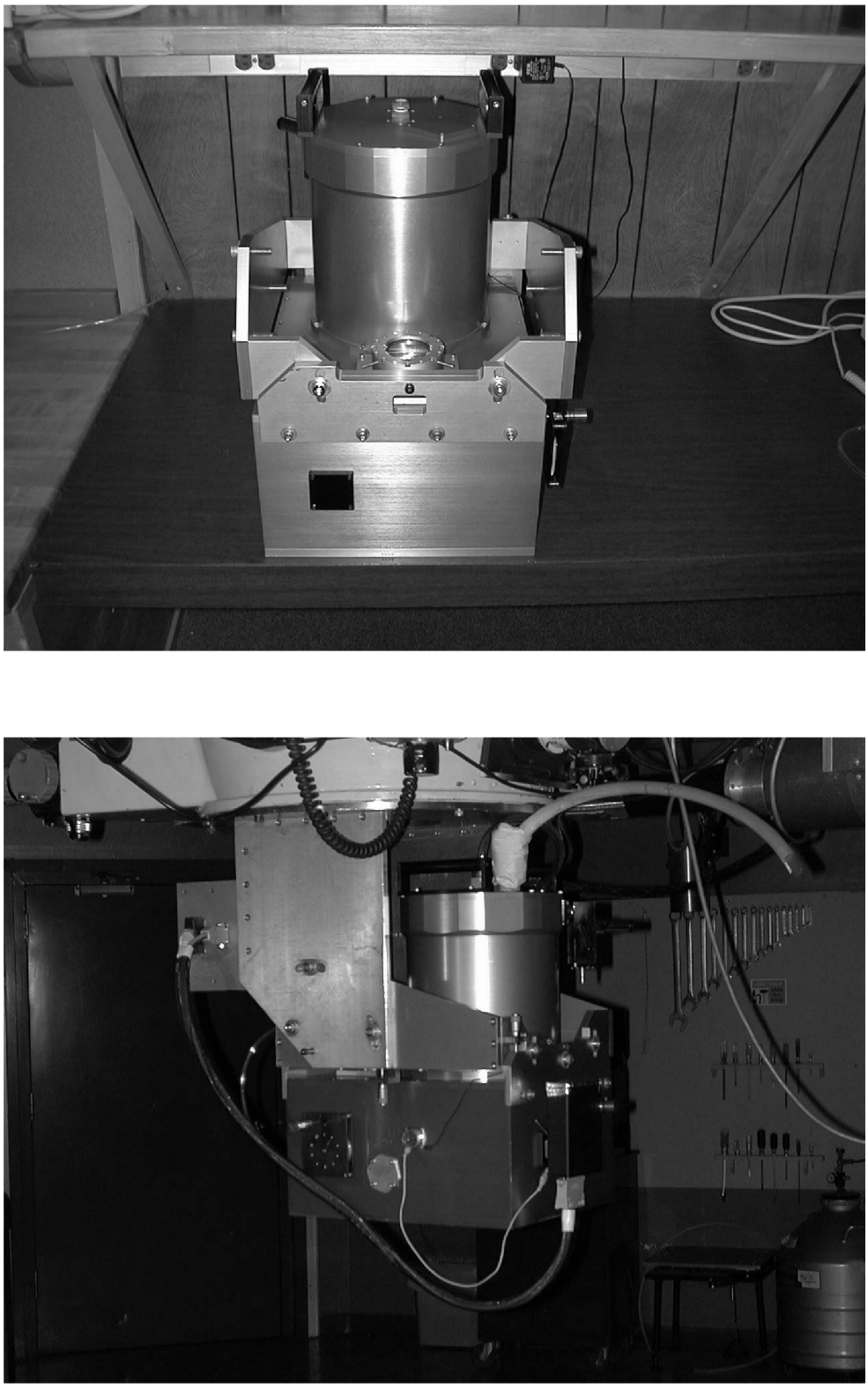

FIG. 1.—PISCES wide-field camera shown on a laboratory bench (*top*) and as mounted at the f/9 Cassegrain focus of the 2.3 m Bok telescope (*bottom*). The up-looking geometry features an achromatic doublet lens system as the vacuum entrance window, seen in the upper image. In the lower image, the array's electronic controller is mounted to the left above the camera. The camera mount can be accurately oriented in two dimensions to position the cold pupil stop for rejection of thermal emission from the edge of the primary mirror, spider vanes, and central obscuration.

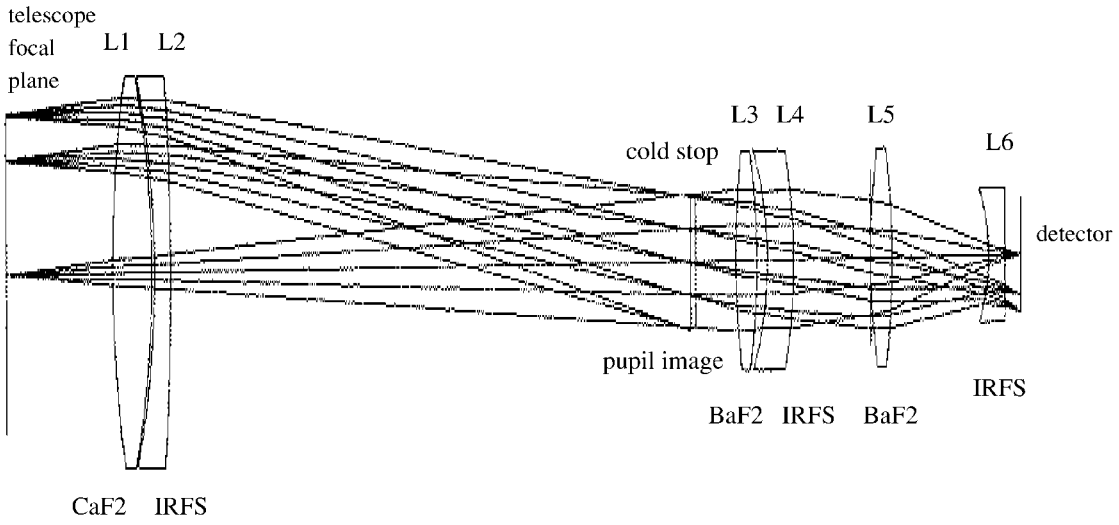

FIG. 2.—Optical configuration of PISCES. The f/9 focal plane of the telescope is reimaged from left to right onto a HgCdTe 1024 × 1024 pixel detector at f/3.3. The initial two lenses form an achromatic doublet (CaF_2, IR fused silica) for reimaging the telescope pupil onto a cold stop. They also form the vacuum-sealed entrance window of the dewar. Standard interference filters are positioned immediately behind the cold stop. Four subsequent lenses (BaF_2, IR fused silica pairs) reimage the initial focal plane onto the detector. All lenses have spherical surfaces and are antireflection coated for ≥98% transmission from 1 to 2.5 μm. Table 1 summarizes the specific optical prescription.

cold stop to block thermally emitting surfaces. The diameter of this stop had to be ≤25 mm to accommodate standard interference filters at that location. Fifth, to reduce costs, the optical elements were made from standard glasses using spherical surfaces which matched standard test plates of the manufacturer. Although the infrared-grade "IRG" glasses from Schott (Oliva & Gennari 1995) would improve optical performance, they were excluded from consideration because of their high cost and lack of availability.

2.2. Optical Design and Manufacture

The optical design utilized Focus Software's ZEMAX program. A multiconfiguration format provided simultaneous designs at two temperatures (300 and 77 K) in order to account for the temperature-dependent refractive indices, spacings, and curvatures of the lens elements. System performance was optimized at 77 K, whereas optical construction and alignment utilized the room-temperature specifications. The optical parameters were optimized for performance at the 2.3 m telescope at 2.2 μm. The final optimization incorporated test plate surfaces available from Janos Technology, Inc.

TABLE 1
PISCES OPTICAL PRESCRIPTION

Lens	Glass	R_1 (mm)	R_2 (mm)	Thickness (mm)	Aperture (mm)
1	CaF_2	109.9	−95.3	14.3	64
2	IR fused silica	−84.5	−212.9	7.0	74
3	BaF_2	84.5	−60.2	10.0	36
4	IR fused silica	−33.1	−47.2	9.8	36
5	BaF_2	63.4	−77.3	8.8	36
6	IR fused silica	−77.3	−18.6	5.3	22

All optical elements except L5 were manufactured by Janos to standard tolerances: ±0.1 mm thickness, 40-20 surface quality, 3′ parallel, ≤5 fringes flatness. Lens L5 required a tighter tolerance (±0.06 mm) in center thickness. Alignment and installation of these optics also did not require special techniques. For example, the aluminum optics tube and spacers, which hold and position the final four lenses, were manufactured to standard machining tolerances of ~25–50 μm.

Figure 3 shows the optical arrangement within the dewar. Located 40 mm below the telescope focal plane, the initial two lenses (CaF_2 and IR fused silica) form an achromatic doublet (diameter = 74 mm) which serves as the dewar's vacuum window and also reimages the telescope's secondary mirror onto a 21 mm diameter cold stop with ≤0.5% blur. The resulting spot size of 80 μm corresponds to 8 mm on the primary mirror. A better pupil image could be obtained with a first lens made from BaF_2 instead of CaF_2. However, the latter was chosen for its superior durability in the ambient environment.

The cold stop strongly suppresses thermal emission from the edge of the primary mirror, central obscuration, secondary mirror baffles, and spider arm supports. This stop was manufactured by Microphoto Inc. from 0.114 mm thick blackened BeCu using an electrochemical process. A 10 position, cooled filter wheel is located immediately behind the cold stop.

The final four lenses (IR fused silica, BaF_2) reimage the telescope focal plane onto the detector with a demagnification of 2.83. This reimaging system is not achromatic, so the tele-

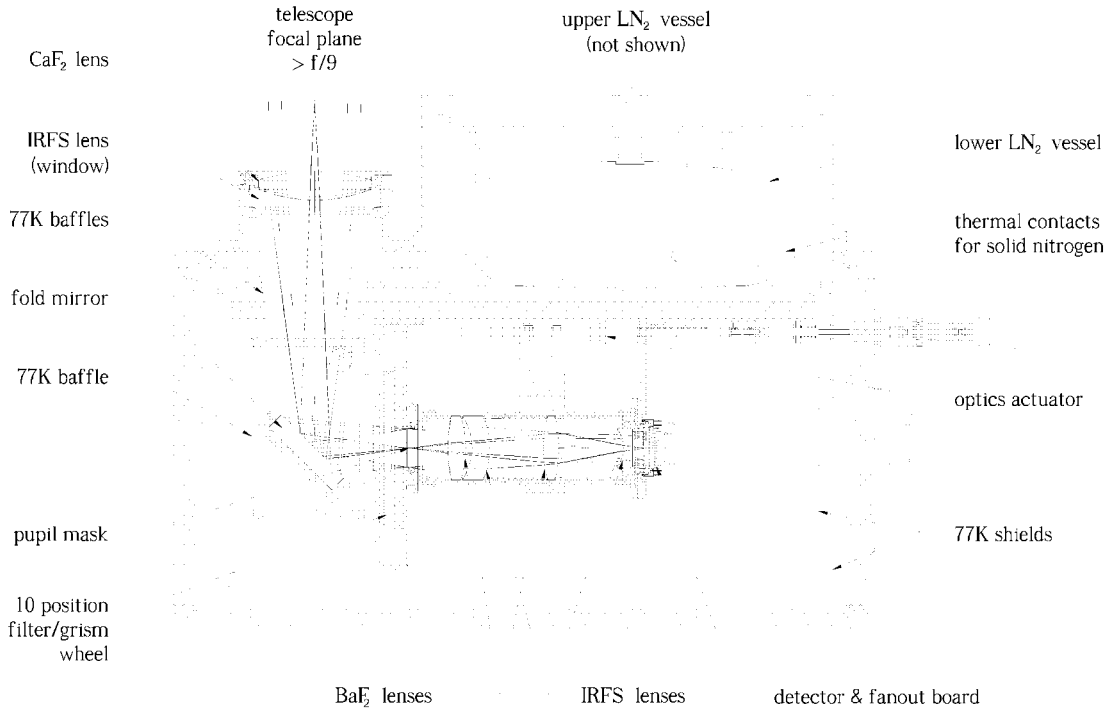

FIG. 3.—Schematic of the PISCES wide-field camera showing the optical configuration including the six refractive elements, filter wheel, pupil stop, and detector.

scope must be refocused when changing filters with a corresponding change in the exact demagnification. The last lens lies just 6 mm above the detector and flattens the final field. To improve image quality, a stop can be placed at L5 to eliminate aberrations associated with the extreme rays at the expense of some vignetting toward the edge of the field.

Figure 4 shows that at the edge of the field of view on the MMT (3′.16) ~85% of the encircled energy from a point source at 2.1 μm lies within a radius of 1 pixel (18.5 μm). Spot size is limited primarily by longitudinal chromatic aberration in the JHK_s bands. This aberration is reduced through the use of BaF_2 and IR fused silica pairs. Optical distortion increases radially outward to a maximum of 3% at the edge of the field. Ghost images are predicted to occur from reflections between the detector and field flattener but at low percentages (≤0.3%) of the original source intensity because of the antireflection coating applied to all lens surfaces for ≥98% transmission from 0.8 to 2.5 μm.

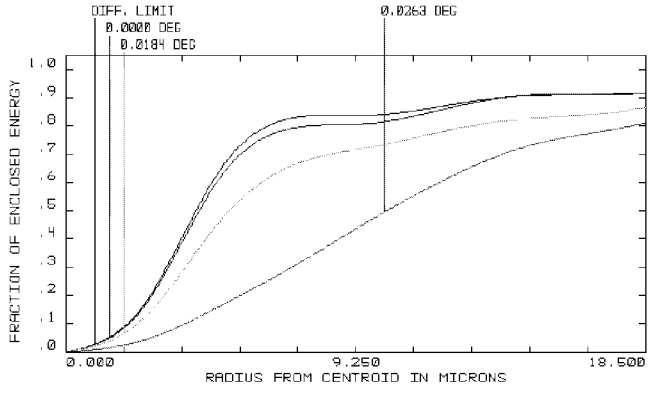

FIG. 4.—Encircled energy vs. field angle at 2.1 μm predicted for the PISCES camera on the 6.5 m MMT. Curves are shown for images located at three field angles corresponding to on-axis (0°.0), 0.7 of full field (0°.18), and full field (0°.026). The uppermost curve corresponds to diffraction-limited performance. About 85% of the encircled energy from a point source lies within a radius of 1 pixel (18.5 μm).

To block the thermal background contributed by the telescope's central obscuration and secondary mirror support structure, the pupil image must be accurately positioned on the cold stop. To accomplish this alignment, a second set of reimaging optics can switch into the optical path to relay images of both the pupil and the cold stop onto the detector with a demagnification of 1.63. These two images can be superimposed accurately by slight tilt adjustments of the dewar on its mount. The pupil-viewing optics are a commercially available triplet, focal length 30 mm, normally used for YAG laser focusing from OptoSigma Corporation. The original mounting cell was enlarged to prevent the lenses from cracking because of differential thermal contraction upon cooling.

Figure 5 shows pupil images obtained on the 6.5 m MMT (f/9) in the K_s band, showing thermal emission from the central obstruction, secondary spider support vanes, and mirror cell around the edge of the primary mirror. The inner bright and

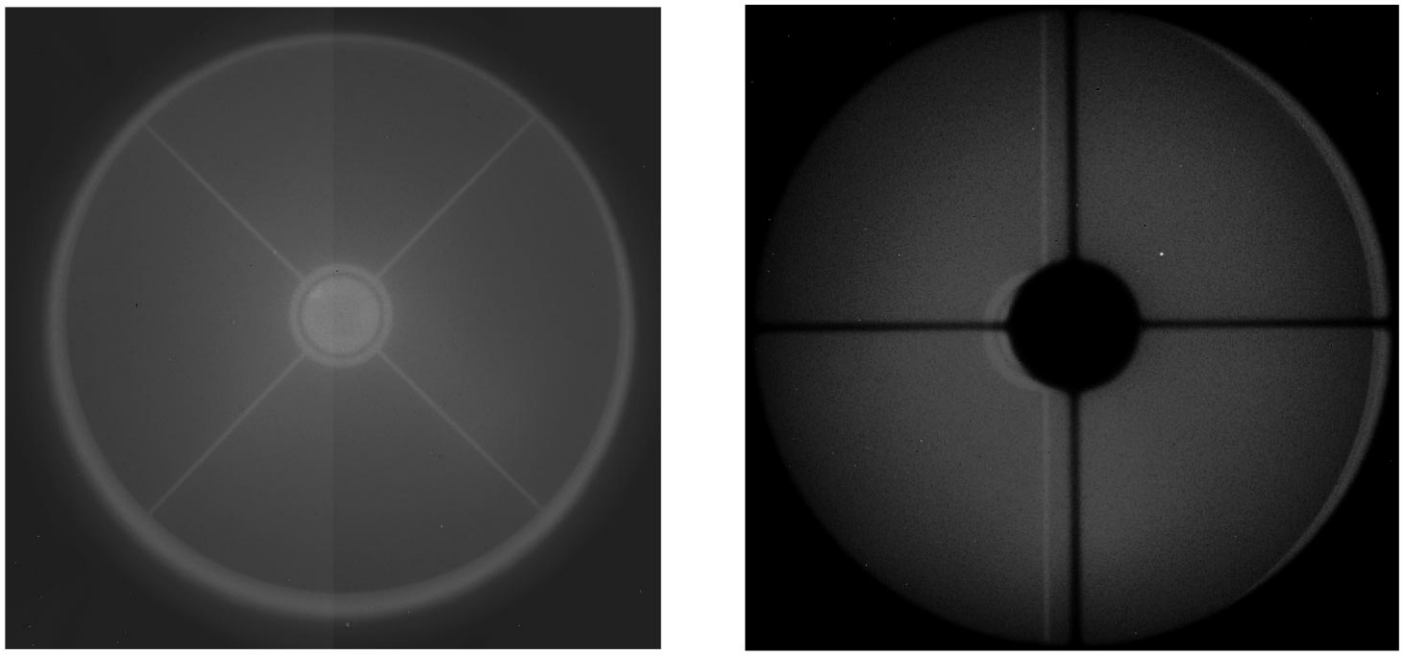

FIG. 5.—Pupil images of the 6.5 m MMT (f/9) in the K_s band without (*left*) and with (*right*) a cold pupil mask installed in the dewar. The main part of these images shows the relatively cold sky after reflection from the primary and secondary mirrors. The left-hand image also shows thermal emission from the telescope's central obscuration, spider arm supports (50 mm width), and mirror cell around the perimeter of the primary mirror. The dark ring in the center occurs as the sky emission is reflected twice from both the primary and secondary. The inner bright annulus is thermal emission from the cylindrical housing which surrounds the secondary. The right-hand image shows the telescope pupil partially blocked by a cold mask (*in black*). The dewar can be tilted to hide the thermally emitting surfaces completely behind the cold mask.

dark annular rings are a consequence of the small diameter of the central hole (0.898 m) in the primary mirror relative to that of the secondary mirror and its housing. The dark ring occurs as sky emission is reflected twice from both the primary and secondary. The inner bright annulus is thermal emission from the secondary's cylindrical housing which is seen by the detector after reflection from the primary and secondary mirrors. All these emissive features are normally blocked by the cold stop.

2.3. The Dewar

Figure 3 shows a cross-sectional diagram of the PISCES dewar. Originally manufactured by Infrared Laboratories, Inc., for the FASTTRAC tip/tilt correction instrument (Close & McCarthy 1994), the dewar was modified slightly to incorporate the wider field optical design. The up-looking geometry helps limit the number of warm emissive surfaces seen by the detector. The dewar contains two vessels of liquid nitrogen to doubly shield the detector environment and to provide a hold time of 22 hours. Two hand-operated actuators are located on the sides for controlling the filter wheel and interchanging the reimaging optics. When mounted on the telescope, the dewar can be tilted slightly in two dimensions for proper alignment (§ 2.2).

3. THE HAWAII DETECTOR AND CONTROL SYSTEM

The PISCES detector has the performance parameters expected for HAWAII focal plane arrays (Hodapp et al. 1996). With its large, 0″.5, pixels at the f/9 Bok telescope, integration times with PISCES are limited by the detector well depth and the local sky background (15–16 *J*, 13–15 *H*, 12.7–13.7 K_s mag arcsec^{-2}). Using a detector bias voltage of 0.9 V (145,000 electron well depth), typical exposure times are 1–2 minutes for *J* band and 20–60 s for *H* and K_s bands. Since PISCES also uses the f/9 focus at the MMT, the background per pixel should be identical.

The camera's control system includes an array controller from San Diego State University (Leach & Low 2000) with a fiber-optic command/data link connected to a personal computer via the PCI bus. This controller contains a digital signal processor and EPROM combination to generate the bias, addressing, and reset voltages for operating the HAWAII detector at a rate of 3 μs pixel^{-1}. A single frame obtained by a reset-read-integrate-read sequence requires 2.4 s plus the integration time. A preamplifier conditions the voltages from the controller and amplifies the detector outputs. In the controller, the four detector quadrants are read out in parallel and each is digitized to 16 bits. The overall system gain is ~5.7 electrons ADU^{-1}.

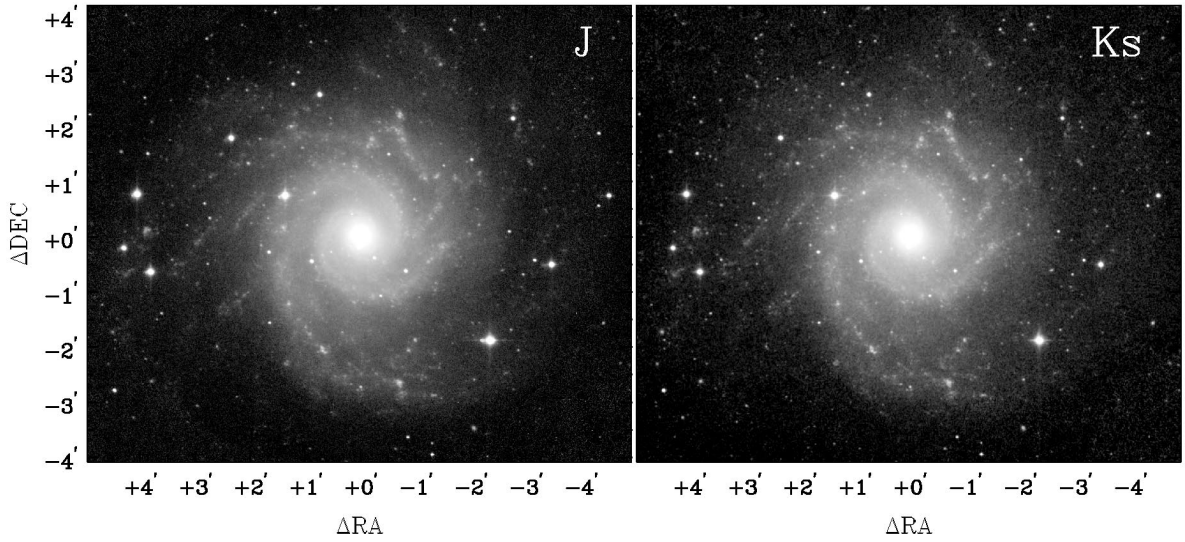

FIG. 6.—*J*- and K_s-band composite images of the Sc galaxy NGC 628 obtained at the 2.3 m Bok telescope. The image dimensions are about 10′ × 8′. North is at top, east to the left. The faintest features (2 σ) have surface brightnesses of about 22.7 *J* mag arcsec^{-2} and 21.4 K_s mag arcsec^{-2}. The brightest sources exhibit ghost images to their immediate left at a level of 0.3% of the original source intensity.

The 16 bit data are transferred at high speed ($\leq 10^7$ pixel s^{-1}) into the computer's random access memory via a PCI-bus interface card (Spectral Instruments, Inc.) and copied in FITS format both to the internal hard drive and also, via Ethernet, to a hard drive on a Sun computer resident at the telescope. The computer is also networked to the Telescope Control System for controlling dithering motions of the telescope and for obtaining information about telescope pointing for insertion in the image headers. A custom C program running under DOS provides a user-friendly environment for controlling detector biases, readout technique, exposure time, and dithering of the telescope.

4. DATA REDUCTION

Some features particular to the HAWAII detectors and the PISCES camera require additional steps in data reduction besides the usual dark subtraction, flat-fielding, and sky subtraction. Our HAWAII array shows a slight offset in intensity between odd and even columns of at maximum 2%, depending nonlinearly on intensity and becoming more severe at extremely short exposure times (<1 s). Such offsets have also been seen in NICMOS3 detectors operated at the University of Arizona and at Infrared Laboratories, Inc. The effect is removed reasonably well by median filtering the images (each quadrant separately) in the column direction over about 100 pixels and scaling each pixel in the original image by the factor needed to bring neighboring odd and even column pixels to the same intensity in the median-filtered image. This method is very similar to scaling entire columns by their intensity offset but more effectively accounts for the offset dependence on local intensity.

An additional effect concerns cross talk between quadrants which leaves "echoes" and associated "tails" in identical positions on the other quadrants. Specifically, each pixel in one quadrant leaves a negative imprint of amplitude ~0.1% in the other quadrants and with an additional negative tail in the readout direction. The tail becomes negligibly small ~150 pixels away from the source. If the source is near an edge of a quadrant, the tail wraps around to the next line in the readout direction. This effect scales linearly with the intensity of the source and can be removed by a simple deconvolution process operating on the full array. A similar phenomenon in HAWAII detectors has been described by Mackay et al. (1998).

Flat fields for the *J* and *H* bands are created by averaging a large number of frames containing only a few objects which are clipped out. In the *K* band this method does not work as well because thermal background can be scattered into the field of view from sources around the dewar window. Flat fields for the *K* band are created during sunset, when the sky intensity is changing rapidly but the thermal component is nearly constant. By subtracting the average of a number of low-intensity sky frames from a stack of high-intensity frames, the thermal component can be removed, leaving a proper flat field similar in shape to the *J*- and *H*-band flat fields. Flat-field accuracy in all bands is typically 2%–4%. All dark-subtracted object frames are divided by the appropriate flat fields.

The geometric distortions are determined by comparing the star positions of a number of densely populated standard-star fields with the accurate positions of these stars in the USNO-A2.0 Catalog (Monet et al. 1998). The transformations are fit by a third-order Legendre function and applied to all flat-fielded science frames. It is not necessary to correct the flux in each pixel for pixel size distortion because the same distortion is

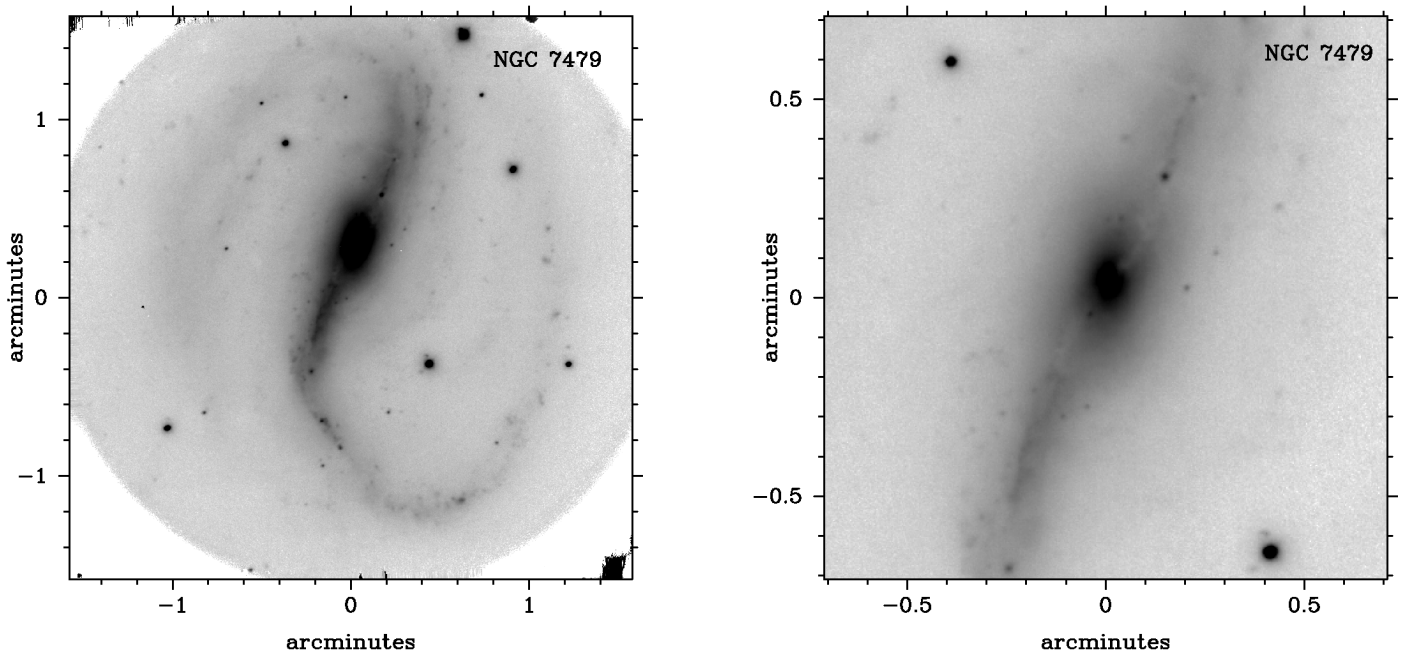

FIG. 7.—*J*-band images of the SBb galaxy NGC 7479 obtained with the 6.5 m MMT. Five 30 s images were co-added after correcting for differential field rotation and tracking errors. Field of view is 3′.16 with an image quality of 0″.74 FWHM. The right panel shows only the inner 1′.4. Image quality was determined by a combination of atmospheric seeing through 1.6 air masses, field rotation, nonoptimized forces on the primary mirror support, and lack of thermal control of the primary mirror. Median seeing at the MMT is expected to produce images with 0″.53 FWHM in the *H* band. This observation is the first wide-field image obtained with the new MMT.

present in the flat field. Correcting for image distortion after flat fielding instead of early in the data reduction pipeline has the benefit that smoothing inherent to regridding occurs just once.

5. ASTRONOMICAL PERFORMANCE

Table 2 summarizes the performance of the PISCES camera as measured at the 2.3 m telescope and as predicted for the 6.5 m MMT. In both cases, PISCES produces subarcsecond spot diameters (FWHM ≤2 pixels) across the full field in the standard *J*, *H*, and K_s infrared photometric bands. Optical distortion is 3% at the field edge and can be completely corrected through standard image processing as described above. Ghost images occur ~8 pixels away from bright point sources at the predicted level (≤0.3%) and have nearly twice the diameter of the point-spread function (PSF). These ghosts do not degrade surface photometry of extended sources. On the 2.3 m telescope, we have measured a telescope emissivity of 5%–7% and throughput (telescope and PISCES) of 50%–55%.

TABLE 2
PISCES PERFORMANCE

Parameter	Measured at 2.3 m Bok	Expected at 6.5 m MMT
Field of view (diameter) (arcmin)	8.5	3.16
Scale (arcsec pixel^{-1})	0.5	0.185
Optical spot (diameter) (pixel)	<1.5	<1.5
Median seeing (*H* band) (FWHM)	1″.2	0″.53
Throughput (%)	50–55	50–55
Emissivity (%)	5–7	5–7
Limiting magnitudes (point sources) (10 σ minute^{-1}) (mag):		
J	19.5	21.7
H	18.5	20.7
K_s	17.6	19.7

Figure 6 shows an example of final mosaicked images using data of NGC 628 obtained with PISCES on the 2.3 m Bok telescope. In the outskirts of the galaxy, these images reach surface brightnesses of 22.7 *J* mag arcsec^{-2} and 21.4 K_s mag arcsec^{-2} in their pixel-to-pixel noise, about 2 σ above the rms sky noise. Integration times were 21 minutes at *J* and 32.5 minutes at K_s. The FWHM of the PSF is typically 1″.2–1″.6.

Overall photometric accuracy has been evaluated by multiple observations of standard-star fields during the course of a photometric night. Each field typically has two to four standard stars with a range of colors and apparent brightnesses. By observing two such fields at different air masses and in five different locations across the full field of view of the detector, we measure residuals of $\sigma \sim 2\%$–3% in photometric solutions.

5.1. PISCES on the 6.5 m MMT

The 6.5 m diameter primary mirror was installed in the MMT in 1999 March (West et al. 1997), more than doubling its light-

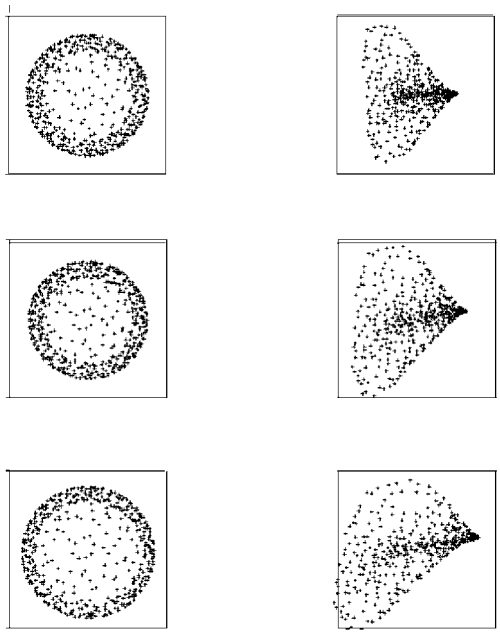

FIG. 8.—Spot diagrams illustrating the expected performance of PISCES for wide-field grism spectroscopy in the *J* (*top*), *H* (*middle*), and *K* (*bottom*) photometric bands. The left-hand column refers to on-axis sources, while the right-hand column refers to an off-axis angle of 0°.025, at the edge of the field of view at the MMT. Even though the light beam is not collimated at the grism, spectra of resolution 500 are produced across the field with Nyquist sampling (2 pixels; 37 μm). To balance focus across the field of view, the on-axis spots are slightly defocused. This ZEMAX simulation incorporates a grism made from As_2S_3 with a wedge angle of 10°.3 and a groove spacing of 41.3 lines mm^{-1}. Spectroscopy in the *J*, *H*, and *K* bands uses orders 5, 4, and 3, respectively.

collecting power as a result of increased collecting area and optical throughput. PISCES can operate at the f/9 focus without any modifications because its optical design was optimized for this f-ratio. In fact, the predicted spot sizes across the field are somewhat improved (~10%) over those at the 2.3 m telescope. The focal plane scale is 0″.185 pixel^{-1} with a resultant field of view of 3′.16 diameter. Because PISCES utilizes the same f-ratio at both the 2.3 m and 6.5 m telescopes, the amount of sky background per pixel will be the same. However, the signal from a point source will increase substantially on the MMT because the collecting area of this telescope is 9 times larger and because the Mount Hopkins site has much better atmospheric seeing as described in the following.

PISCES is well matched to the seeing conditions at the MMT. The best measure of these conditions comes from detailed analyses of image motion by the Steward Observatory adaptive optics group using the original 4.5 m MMT (Lloyd-Hart et al. 1998). Typically, the Fried parameter, r_0, equals 0.9 m at K_s band with second and 10th percentile values of approximately 3–4 m and 2 m, respectively. Extrapolating these values to *H* band, we generally expect FWHM of 0″.53 with a 10th percentile value of ~0″.24. Actual image quality may be even better because of new improvements in thermal management of the telescope optics and of the overall facility. Expected errors in telescope tracking (0″.070) and anticipated wind shake (0″.05 for winds $\leq$11 m s^{-1}) should not degrade the above performance significantly. Based on the expected Fried parameter and on the discussion of Martin (1987), the tip/tilt component of atmospheric seeing should be 0″.15 (two-dimensional), the removal of which would yield only slight improvements in the median FWHM.

Figure 7 shows the first wide-field image obtained with the 6.5 m MMT on 2000 September 6 during an initial engineering run. Using PISCES in the *J* band, five 30 s images of the galaxy NGC 7479 were co-added after correcting for differential field rotation and tracking errors. The resulting image quality was 0″.74 FWHM and was affected by a combination of atmospheric seeing through 1.6 air masses, field rotation, nonoptimized forces on the primary mirror support, and lack of thermal control of the primary mirror.

5.2. Comparison to Other Cameras

One measure of the performance of a wide-field camera is its "survey efficiency," defined as the square of the product of field of view and telescope diameter (Elston 1998) under identical atmospheric seeing. Equipped with a 1024 × 1024 pixel detector, PISCES achieves a survey efficiency of 385 m^2 arcmin^2 on both the 2.3 m Bok telescope and the 6.5 m MMT. This value exceeds the 275 m^2 arcmin^2 achieved by the Near Infrared Imager on the 8.1 m Gemini telescope. With a 2048 × 2048 pixel detector, FLAMINGOS (Elston 1998) has a higher survey efficiency, 1514 m^2 arcmin^2, on the Mayall 3.8 m telescope. Nevertheless, PISCES gains in other important performance parameters such as higher spatial resolution, 0″.18 (MMT) versus 0″.3 pixel^{-1}, and possibly optical throughput because it has fewer optical elements (six vs. nine).

5.3. Larger Format Detectors

The optical design for PISCES is directly applicable to wider field cameras using even larger format detector arrays. For example, ray-tracing indicates that the present design can be expanded a factor of 2 to accept a 2048 × 2048 pixel detector at 0″.5 pixel^{-1} on the 2.3 m telescope at f/9. After reoptimization of the lens surfaces, this solution provides good image quality (rms spot size $\leq$2 pixels; 18.5 μm pixels) over a 17′ × 17′ field of view. Optical distortion at the field edge remains ~3%. Therefore, this design serves as an example for future wide-field cameras featuring low cost, high throughput, and minimal ghost images.

6. FUTURE GRISM SPECTROSCOPY

PISCES could be equipped with a grism for low-resolution (R = 200–500) single-object and multiobject spectroscopy (Finn & McCarthy 2000). This configuration would greatly

facilitate the spectral classification of individual galaxies in clusters and in quasar environments as well as very low mass stars and brown dwarfs in young clusters.

The spectroscopic design can utilize the existing optics with a grism located immediately behind the cold pupil stop with order-sorting filters in the existing 10 position filter wheel. Although the incident light is not collimated at the grism, grisms of high-index material with narrow wedge angles can produce Nyquist sampled (2 pixel) spectra of resolution 500 across most (90%) of the field. For example, Figure 8 shows the spot diagrams expected for a grism made from As_2S_3 ($n = 2.438$ at $\lambda = 1.53$ μm) with a wedge angle of 10°.3 and a groove spacing of 41.3 lines mm^{-1}. This device allows spectroscopy in the *J*, *H*, and *K* bands using orders 5, 4, and 3, respectively. Silicon grisms (Ge et al. 2000; Keller et al. 2000) are also attractive possibilities.

A single or multiple slit mask would be placed at the focal plane, located 40 mm above the entrance to the dewar. With an extension to the dewar, this mask could be cooled thermoelectrically to reduce its thermal emission in the *K* band. The plate scale at the MMT focal plane is 3″.5 mm^{-1}, so the 0″.36 slits needed to achieve a spectral resolution of 500 will be 0.1 mm wide. Individual slit masks of this quality can be manufactured by electrochemical and micromachining techniques. An attractive alternative which provides more versatility is a microshutter assembly (Kutyrev et al. 1999). In either case, the small slits at the MMT would require a guiding capability to keep the object centered on the slit. Autoguiding and autofocusing are possible by adding a movable probe assembly such as that planned for the ARIES instrument (Sarlot et al. 1999).

The authors are grateful for the important engineering contributions provided by Elliott Solheid and Mitch Nash (cryomechanical), Roland Sarlot and Jim Burge (optical), Frank Low (detector), Ken Salvestrini and Bob Leach (detector control), and Matt Cheselka (software). The HAWAII detector and electronic controller were purchased by the Air Force Office of Scientific Research through grant F49620-96-1-0285. The PISCES project was also briefly supported by the National Science Foundation through grant NSF 96-23788. R. F. acknowledges support from NASA training grant NGT5-50283. Support for R. S. de Jong was provided by NASA through Hubble Fellowship grant HF-01106.01-98A from the Space Telescope Science Institute, which is operated by the Association of Universities for Research in Astronomy, Inc., under NASA contract NAS 5-26555.

REFERENCES

Close, L., & McCarthy, D. W. 1994, PASP, 106, 77
Elston, R. 1998, Proc. SPIE, 3354, 404
Finn, R. A., & McCarthy, D. W. 2000, Proc. SPIE, 4008, in 759
Ge, J., et al. 2000, BAAS, 195.8715
Hodapp, K. W., et al. 1996, NewA, 1, 177
Keller, L., Jaffe, D., Ershov, O., Benedict, T., & Graf, U. 2000, Appl. Opt., 39, 1094
Kozlowski, L. J., et al. 1994, Proc. SPIE, 2268, 353
Kutyrev, A. S., et al. 1999, BAAS, 195.8607
Leach, R., & Low, F. 2000, Proc. SPIE, 4008, in 337
Lloyd-Hart, M., et al. 1998, ApJ, 493, 950
Mackay, C. D., Beckett, M. G., McMahon, R. G., Parry, I. R., Piche, F., Ennico, K. A., Kenworthy, M., Ellis, R. S., & Aragon-Salamanca, A. 1998, Proc. SPIE, 3354, 14
Martin, H. M. 1987, PASP, 99, 1360
Monet, D., et al. 1998, USNO-SA2.0 Catalog (Washington, DC: USNO)
Oliva, E., & Gennari, S. 1995, A&AS, 114, 179
Sarlot, R., McCarthy, D., Burge, J., & Ge, J. 1999, Proc. SPIE, 3779, 274
West, S. C., et al. 1997, Proc. SPIE, 2871, 38